Sensors and Actuators B 251 (2017) 1059–1067

Contents lists available at ScienceDirect

Sensors and Actuators B: Chemical

journal homepage: www.elsevier.com/locate/snb

Enhancing sensitivity of photonic crystal fiber interferometric humidity sensor by the thickness of SnO_2 thin films

Diego Lopez-Torres[a,*], Cesar Elosua[a,b], Joel Villatoro[c,d], Joseba Zubia[c], Manfred Rothhardt[e], Kay Schuster[e], Francisco J. Arregui[a,b]

[a] Nanostructured Optical Devices Laboratory, Electric and Electronic Engineering Department, Public University of Navarre, Edif. Los Tejos, Campus Arrosadía, 31006 Pamplona, Spain
[b] Institute Of Smart Cities (ISC), Centro Jerónimo de Ayanz, Campus Arrosadia, 31006 Pamplona, Spain
[c] Department of Communications Engineering, Escuela Técnica Superior de Ingeniería de Bilbao, University of the Basque Country, Bilbao 48049, Spain
[d] IKERBASQUE, Basque Foundation for Science, Bilbao, Spain
[e] Leibniz Institute of Photonic Technology (IPHT), Albert-Einstein-Strasse 9, 07745 Jena, Germany

ARTICLE INFO

Article history:
Received 15 October 2016
Received in revised form 19 May 2017
Accepted 23 May 2017
Available online 25 May 2017

Keywords:
Photonic crystal fiber
Interferometer
Sputtering
Thickness
Humidity sensor
Evanescent field

ABSTRACT

In order to improve the sensitivity of an interferometric humidity sensor based on a photonic crystal fiber with a sputtered SnO_2 nanocoating, a study of the effect of its thickness on the sensitivity is presented in this paper. Sensors with coatings of different thickness were performed by applying distinct sputtering times in order to obtain an optimal thickness: the resulting nanofilms ranged from 470 to 1800 nm. Sensors were tested increasing the relative humidity from 20% to 90%, finding that the thickness was a key parameter which has to be optimized at nanometer scale to get the best sensitivity. The study points that there is an optimal thickness and higher or lower thicknesses worsen the sensitivity of the sensor. The optimal sensor showed a humidity resolution of 0.067%HR, a wavelength shift of 67 nm and a negligible sensitivity with the temperature.

1. Introduction

A high number of papers have been published in the field of optical fiber optics in the last decades. This fact is due to that fiber optic sensors have several advantages over other devices such as electromagnetic immunity, light weight, low transmission losses in the communication window, low cost or wavelength multiplexing, making very interesting its use in many applications [1–4].

In this context, new optical fibers have been developed in order to improve the characteristics of the traditional fibers such as the guidance of the polarization, unprecedented dispersion or non-linear properties. It is the case of Photonic Crystal Fibers (PCFs), also called holey fibers, which contain arrays of tiny air holes along their structure [5–7]. This kind of fibers has attracted an intense research activity because of the possibility of fabricating new optical fiber sensors; devices based on the evanescent field interaction in the holes inside these microstructured fibers is an example [8].

The holey structure of photonic crystal fiber (PCF) allows to detect many parameters such as gases [6], volatile organic compounds (VOCs) [9], temperature [10], strain [11] or humidity [12]. To enable the interaction, the holes of the PCF are collapsed making possible that the modes of the fiber can interact with the evanescent field and with the environments [13]. Previous papers show interesting results in these fields which encourage to work in them as is the case of humidity sensors [14,15]. The measurement of humidity is required in a range of areas, including meteorological services, chemical or medicine industry, food and beverages processing industry, civil engineering, air-conditioning, horticulture, and electronic processing [16,17]. These sensors, compared with their conventional electronic counterparts, offer specific advantages such as the possibility to work at high relative humidity values avoiding the risk of short circuit or corrosion resistance, among others mentioned above.

Most of these fiber optic humidity sensors work on the basis of a hygroscopic material coated over the optical fiber to modulate the

Abbreviations: PCF, photonic crystal fiber; PCF-I, photonic crystal fiber interferometer; SMF, single mode fiber; LMR, Lossy mode resonances; RH, relative humidity; OSA, optical spectrum analyzer.

* Corresponding author.
E-mail addresses: diego.lopez@unavarra.es (D. Lopez-Torres), cesar.elosua@unavarra.es (C. Elosua), agustinjoel.villatoro@ehu.eus (J. Villatoro), joseba.zubia@ehu.es (J. Zubia), kay.schuster@leibniz-ipht.de (K. Schuster), parregui@unavarra.es (F.J. Arregui).

http://dx.doi.org/10.1016/j.snb.2017.05.125
0925-4005/

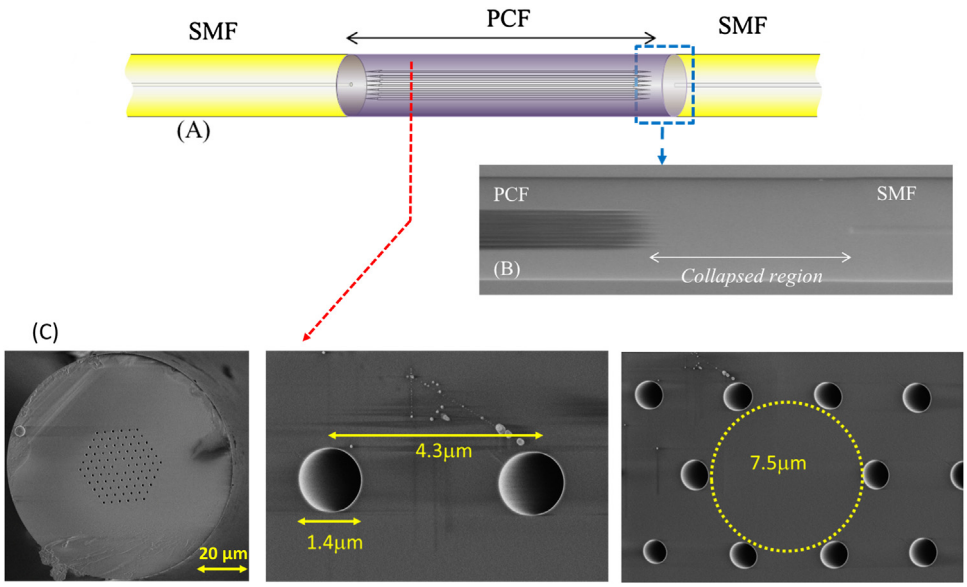

Fig. 1. (A) Scheme of the photonic crystal fiber interferometer (PCF-I): (B) Detail of the splice between PCF and SMF showing the collapsed region of the PCF: (C) Cross section, geometry and dimensions of the PCF used in this work.

light propagating through the fiber. In [18], a relative humidity sensor based on an agarose coating is reported. This study shows that the technique used to deposit this type of materials, dip-coated, does not ensure a repeatable coating in different sensors. Because of this, it is necessary to monitor the spectral shift during the coating process to achieve an optimal thickness for the coating. For this reason, in this paper the use of a hygroscopic material that can be deposited by an electrostatic self-assembly onto the fiber with a repeatable thickness is proposed as a good alternative in the future. In [19], this subject is tackled with very interesting results using the Layer-by-Layer nanoassembly technique [20].

With the aim to improve the sensitivity of previous devices, the current work proposes an interferometric humidity sensor based on a PCF with a sputtered semiconductor nanocoating (tin oxide, SnO_2) [21]. SnO_2 is highly sensitive to changes on the humidity [22] and, when used onto optical fiber, it does not have to be heated to operate. Among different methods to deposit it, sputtering technique allows nanofilms to be fabricated with a high uniformity, reproducibility and with short construction times [23]. Furthermore, the nanofilm thickness can be controlled at nanometer scale. This feature is critical in the case of sensors based on the interaction of the evanescent field with the coating because the thickness should be always below its penetration depth [18,19]. Moreover, thanks to the interferometric nature of the proposed device, the growing of the coating can be monitored on real time by registering the transmission spectra of the sensor and observing any red or blue shift. The resulting sensor characterization can be also expressed in terms of spectral shift, which is more robust than intensity based measurements.

The sensor developed in this paper improves the sensitivity and the wavelength shift of previous works, has a good repeatability and it is relatively easy to made. Also, to our knowledge this is the first time that a SnO_2 nanocoated has been deposited by means of sputtering technique on a PCF as humidity sensor.

2. Experimental details

2.1. Sensing material

SnO_2 has various specific and unique properties, which make this material very useful for many applications [24]. The structure of SnO_2 is an isotropic polar crystal which crystallises in tetragonal rutile structure. The unit cell contains six atoms (2-tin and 4-oxygen, respectively). Each tin atom is at the center of six oxygen atoms placed at the corners of a regular slightly deformed octahedron [25,26]. Thanks to this geometry, the interaction with water molecules is possible but in different ways depending on the temperature. The majority of metallic oxides need to work at temperatures higher than 150 °C [27] but this paper proposes to perform the study at room temperature (25 °C). At this temperature, below 60 °C, water molecules interact with SnO_2 by means of physisorption (the adsorption with the least possible interaction due to the dipole/dipole interactions) [26]. Based on these properties and knowing that SnO_2 is highly sensitive to relative humidity changes, chemically stable and it can be deposited by sputtering technique, it was chosen as sensing material.

2.2. Theoretical background of the PCF-I

The dimensions of the PCF used are shown in (Fig. 1). The air holes pattern are distributed in a hexagon (with a radius of 20 µm) centered at core fiber: each hole has a diameter of 7.5 and the distance between two neighbor holes is 4.3 µm (Fig. 1C). The interferometric sensor was built by splicing 1 cm of PCF between two standard single mode fibers (SMF) (Fig. 1A). Due to the splicing, the voids of the PCF were collapsed completely along the two transitions SMF-PFC-SMF [28]. These transitions were named micro-hole collapsed region (Fig. 1B).

To understand how the interferometer works, it is necessary to analyze the optical signal when it gets into the interface between SMF and PCF and vice versa. At this point, part of the fundamental SMF mode is coupled to the PCF cladding modes which are affected by the external refractive index. The propagation constants of PCF cladding modes are different and consequently, the cladding modes accumulate a phase difference as they propagate along the PCF section. Once these cladding modes reach the second PFC-SMF transition, they interfere with the remaining fundamental SMF mode, producing an interferometric response. Fig. 2 shows a design of the light beam to make easier the understanding. This is the transduction mechanisms of the device and it is based on a Mach Zehnder interferometer [29].

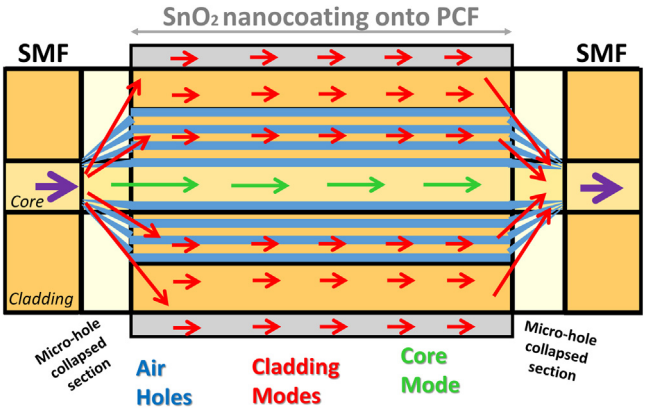

Fig. 2. Operating mechanic of the PCF-I. The arrows show the behavior of the cladding and core modes trough the PCF; in blue are drawn the holes of the PCF and in black the micro-hole collapsed sections; along the PCF the SnO_2 nanocoating is represented with a grey rectangle. (For interpretation of the references to colour in this figure legend, the reader is referred to the web version of this article.)

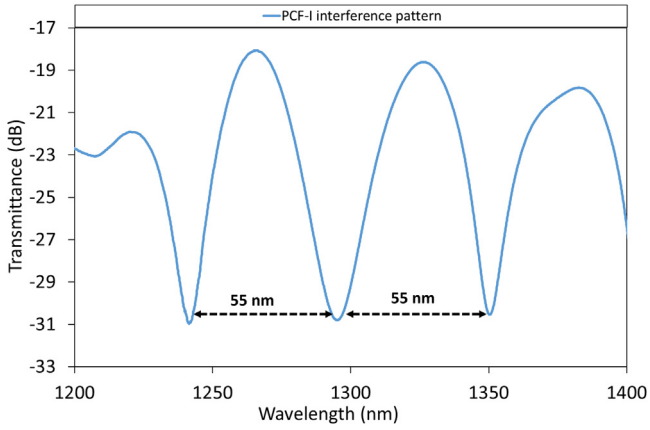

Fig. 3. Interference pattern of the PCF-I from 1200 nm to 1400 nm with a difference between peaks of 55 nm.

Fig. 3 shows the interferometric response obtained before the deposition of the SnO_2 thin film. It can be seen that the transmission of the PCF-I exhibits a series of periodic maxima and minima with a period of 55 nm. The transmission spectrum of the interferometric pattern can be expressed with the next mathematical formula [30]:

$$T(\lambda) = I_{co}(\lambda) + I_{cl}(\lambda) + 2[I_{co}(\lambda) I_{cl}(\lambda)]^{1/2} + \cos\left(2\pi \Delta n_{ef} L/\lambda\right)$$

where I_{co} and I_{cl} are the intensities of the cladding and core modes, L is the length of the PCF-I segment and λ is the wavelength of the guided light. These parameters are constant but the term $\cos(2\pi Dn_{ef} L/\lambda)$ changes, specifically Δn_{ef}: this parameter is the difference between the refractive index of core and the effective refractive index of cladding modes. In our case, the effective refractive index of cladding modes is influenced by the change in the effective refractive index of the nanofilm as well as by the working wavelength. This theory can be applied if the nanofilm thickness is below the penetration depth of the evanescent field: otherwise, the nanofilm acts as an infinite medium because any thickness increase does not modify the effective refractive index of the cladding. Due to this fact, it is necessary to make a study with different nanofilm thicknesses in order to obtain an optimal value.

2.3. Experimental set up and instrumentation

As it can be observed in Fig. 4, the set up used for the construction of the SnO_2 thin film was performed in transmission mode. A multi-LED light (HP83437A) source was used to illuminate a standard SMF (Corning SMF-28) whose emission spectrum range was from 1200 nm to 1600 nm. A Pulsed DC-Sputtering System (Nadetech Inc.) was used to fabricate the SnO_2 thin film and an optical spectrum analyzer (OSA-HP86142), controlled by a computer, was used to analyze the PCF-I interferometric response during the construction process as well as during the characterization of the sensor.

Fig. 4 also shows the set up used to the interrogation of the humidity response of the sensor. This set up was similar to the previous one only replacing the Pulsed DC-Sputtering System instead of the climatic chamber (Angelantoni, CH 250) where de PCF-I was located. The sensor humidity response was performed placing the PCF-I into the climatic chamber where the humidity was increased/decreased from 20% to 90% RH at a constant temperature of 25 °C.

2.4. Construction of the nanofilm

The PCF-I was placed into the vacuum chamber of the sputtering machine, where it was coated with SnO_2. An advantage to use a DC-Sputtering System is that the material is deposited homogenously around the entire surface of the fiber avoiding the necessity to rotate it. The two SMF pigtails were placed in the sputtering machine through wall bushings which ensured the vacuum, so that the transmission spectrum could be tracked in real time. In this way, an increase in the nanofilm thickness should produce a red shift in the interference pattern, making possible to follow the growing as well as preparing PCF-I in a reproducible manner.

The SnO_2 target, 99.99% of purity, was purchased from ZhongNuo Advanced Material Technology Co. The sputtering machine was set to a power of 90 mW, a current of 140 mA and a chamber pressure of 6×10^{-2} mbar. Four sensors were carried out with different thin films and different construction times: in every case, the distance between the SnO_2 target and the PCF-I was 5 centimeters. The resulting thickness of the nanofilm is determined by the construction time in such a way that the thickness increases as the time passes. In order to confirm that the nanofilm construction process is reproducible, three different constructions (with a deposition time of 5 min) were carried out on three different days with the same construction parameters mentioned above. The resulting nanofilm thicknesses (337 nm, 334 nm and 328 nm, respectively) were measured with a quartz crystal microbalance (QCM) located at a 9 cm from the SnO2 target. Consequently, a standard deviation of 3.74 nm (less than 1.15%) was obtained, confirming in this manner that the sputtering technique can be considered highly reproducible. Several authors have studied the effect of post processing in metallic oxide, such as heat curing, with interesting results but this effect will be studied in future works due to the main objective of this paper is to study the feasibility of the humidity sensor [31].

3. Study of the optimal nanofilm thickness

First of all, a sputtering construction of 100 min was carried out with the intention of studying the behavior of the PCF-I during construction in terms of the wavelength shift. Fig. 5A shows the evolution of the PCF-I peaks along the construction time. The resulting spectrums during the 100 min sputtering were recorded every minute: all of them were displayed in a 2D graph. Every spectrum was represented in the vertical axis and their respective magnitudes (expressed in dB) were indicated by a color map. Each peak of

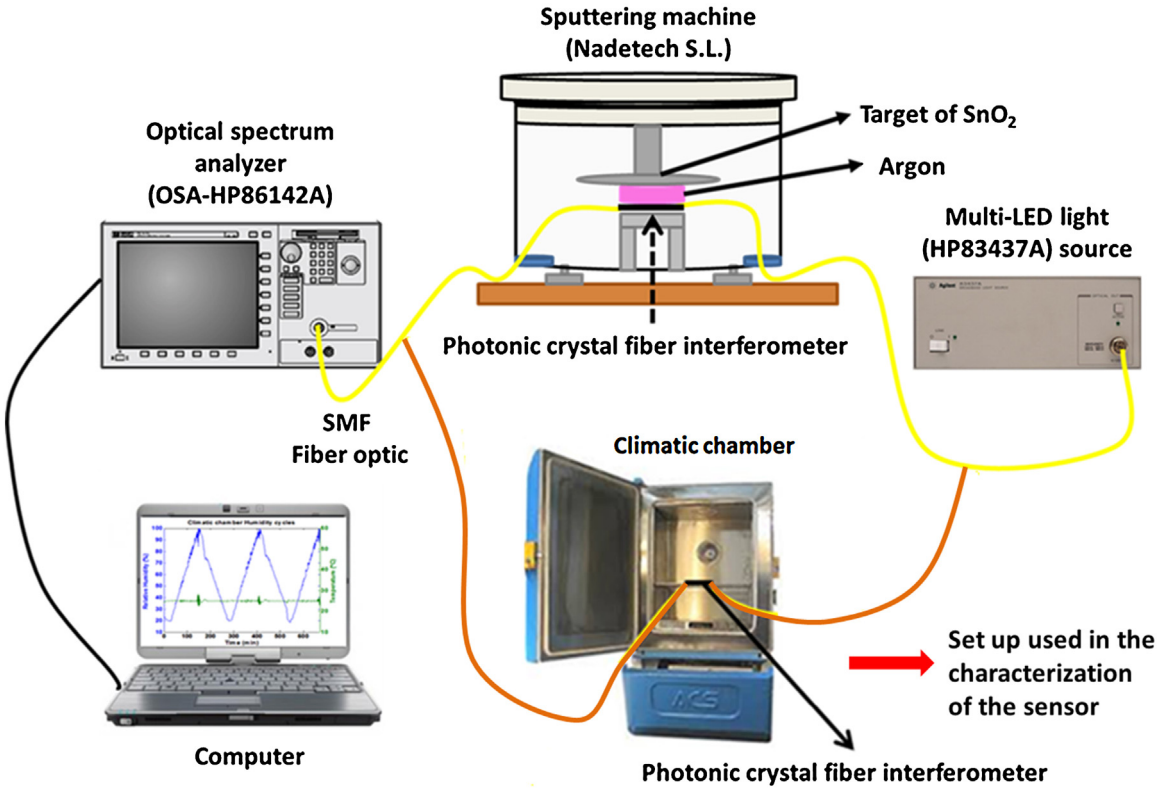

Fig. 4. In yellow, the transmission set up used to monitor the deposition process based on sputtering method; in orange, the transmission set up used to characterize the response of the sensor towards humidity. (For interpretation of the references to colour in this figure legend, the reader is referred to the web version of this article.)

the interference pattern has associated a wavelength shift. For certain areas for the graph, the shifts describe a slope: this parameter can be used to determine the optimum point to stop the construction [19]. At the point where the slope is high, small changes in the refractive index of the coating will give high spectrum shifts, or in other words, will yield into a high sensitivity.

As it can also be appreciated in Fig. 5A, there are zones (indicated by dashed black circles) where the interference pattern disappears. It is due to the presence of a certain electromagnetic resonance known as Lossy Mode Resonance (LMR) [32]. Briefly, an LMR consists of the coupling of the light traveling through the core to the cladding when certain boundary conditions (related with the refractive index and the thickness of the coating) happen. In the case of the PCF-I, when these conditions are fulfilled, the core mode along the PCF segment loses its intensity, in such a way the interference between cladding modes and it is negligible at the second collapsed region [33]. As it can be noticed in Fig. 5B, LMRs appear at 20 min, 40 min, 60 min and 80 min during the sputtering process. It is critical to avoid this phenomenon to obtain a proper interferometric pattern. In light of these results, the sputtering time was limited to 20 min.

It is also noticeable that there is not slope change and therefore no wavelength shift when the construction last longer than 40 min. This is because sputtering times above this value yield to a thickness higher that the penetration depth of the evanescent field: in this manner, the coating acts as infinity medium. As a consequence, no shift in the interferometric pattern is observed beyond this time.

With the aim to locate the point which the highest peak slope, the evolution of the spectral shift during the first 20 min of construction process were studied in details. To make its evaluation easier, three different sections were considered (they are delimited in Fig. 5B with a vertical dashed black line), each one with a specific slope (red shift in every case):

- Up to the first 10 min the total shift is 25 nm, and it is the lowest observed.
- Between 10 and 15 min the slope of the peaks shift was increased up to 53 nm
- Beyond 15 min the total wavelength shift is 79 nm but as the deposition time gets close to 20 min, the amplitude of the peaks tends to decrease and finally, the interferometric pattern disappears. It is due to the presence of a zone where the interference pattern disappears, and consequently this period of time is not the best option to stop the construction

Taking these considerations about the sputtering time into account, four sensors were performed with different times: the first two sensors with a construction time of 5 and 10 min, the third one with 15 min and the last one with 20 min. The corresponding thicknesses for each one were measured by Scanning Electronic Microscope (SEM): 470 nm, 800 nm, 1150 nm and 1800 nm, respectively.

As it can be seen in Fig. 5C, the spectrum of the PCF-I showed several peaks with different amplitudes and transmittances. To make the study easier, only one peak of them was selected although every peak had its own wavelength shift; the peak centered at 1295 nm (in Fig. 5C is highlighted by a red circle). This peak was selected because it was the narrowest and had the highest dynamic range. The spectral shifts of this peak with the four different thicknesses are showed in Fig. 6. In each case, initial pattern is plotted in blue (left vertical axis) and the shifted one is drawn in orange (right vertical axis). The sensor with a construction time of 20 min showed the highest wavelength shift but it had some drawbacks: as it can be seen in Fig. 6.D, the dynamic range of this peak was reduced considerably because of the proximity of the LMR. Due to this fact, a small red wavelength shift when it was exposed towards humidity changes would cause the loss of the interference pattern. Taking it

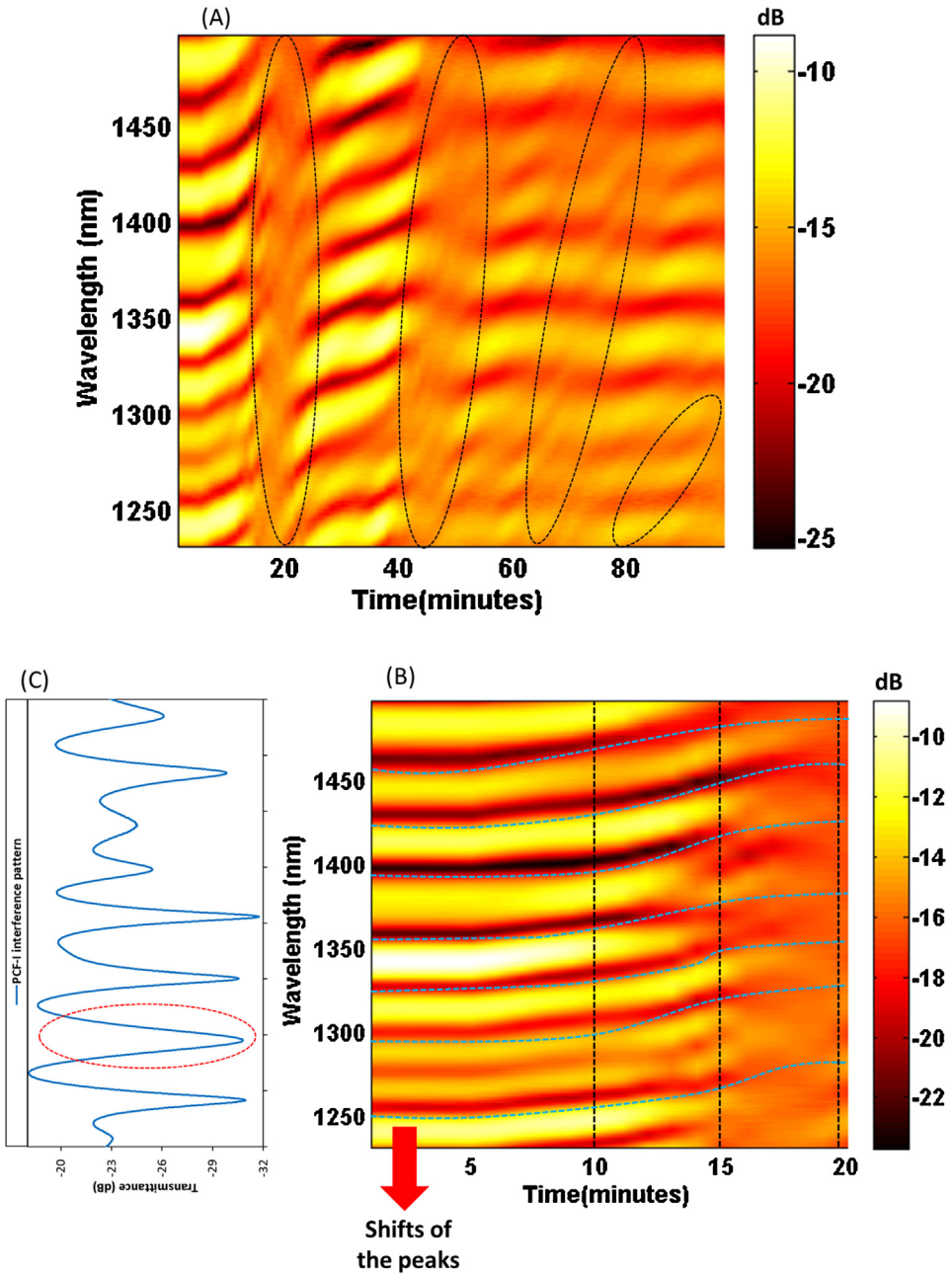

Fig. 5. (A) Spectra red shift observed along the construction process of the nanofilm: a black dashed circle indicates the zones where the interference pattern disappears: (B) Detail of the first 20 min to show three different sections with distinct spectral shifts: the dashed turquoise blue lines show the wavelength shifts of the different peaks of the PCF-I spectrum along the first 20 min of the construction process (C) Transmission spectra of the PCF-I which the peak selected for the study in a red dashed circle. (For interpretation of the references to colour in this figure legend, the reader is referred to the web version of this article.)

into consideration, it was decided to choose the sensor prepared with 15 min sputtering time (and a 1150 nm coating thickness): the shift produced by the coating is 53 nm and at that point, the high slope and the narrower and deeper valley guaranteed a high sensitivity and a better way to register spectral shifts.

4. Results and discussion

The behavior of the four sensors towards humidity was studied by placing them in a climatic chamber where relative humidity was varied from 20% to 90% RH while the temperature was kept constant to 25 °C. The shifts observed for the peak initially located at 1295 nm for each sensor are displayed in Fig. 7A. It can be observed that the highest shift is obtained for the sensor with a thickness of 1150 nm, specifically, 67 nm: it confirms the hypothesis exposed before about the optimal sputtering time. To our knowledge, this wavelength shift improves the previous results reported in other papers [34,35]. These experimental results showed a sensitivity of 0.96 nm/HR% for this sensor and a relative humidity resolution of 0.067%HR (with an OSA resolution of 0.06 nm). Lower sensitivities were obtained for the rest of thicknesses, 0.23 nm/HR% (480 nm); 0.31 nm/HR% (800 nm); and 0.19 nm/HR% (1800 nm), respectively. It is remarkable that for a lower thickness, the total spectra shift was lower (16 nm and 22 nm, respectively); this is because of the nanofilm thickness is thinner than the one of the optimized sensor and a smaller part of the evanescent field interact with it. Regarding to the sensor with a thickness of 1800 nm, the wavelength shift was 13 nm. The reason of the low wavelength shift has been exposed

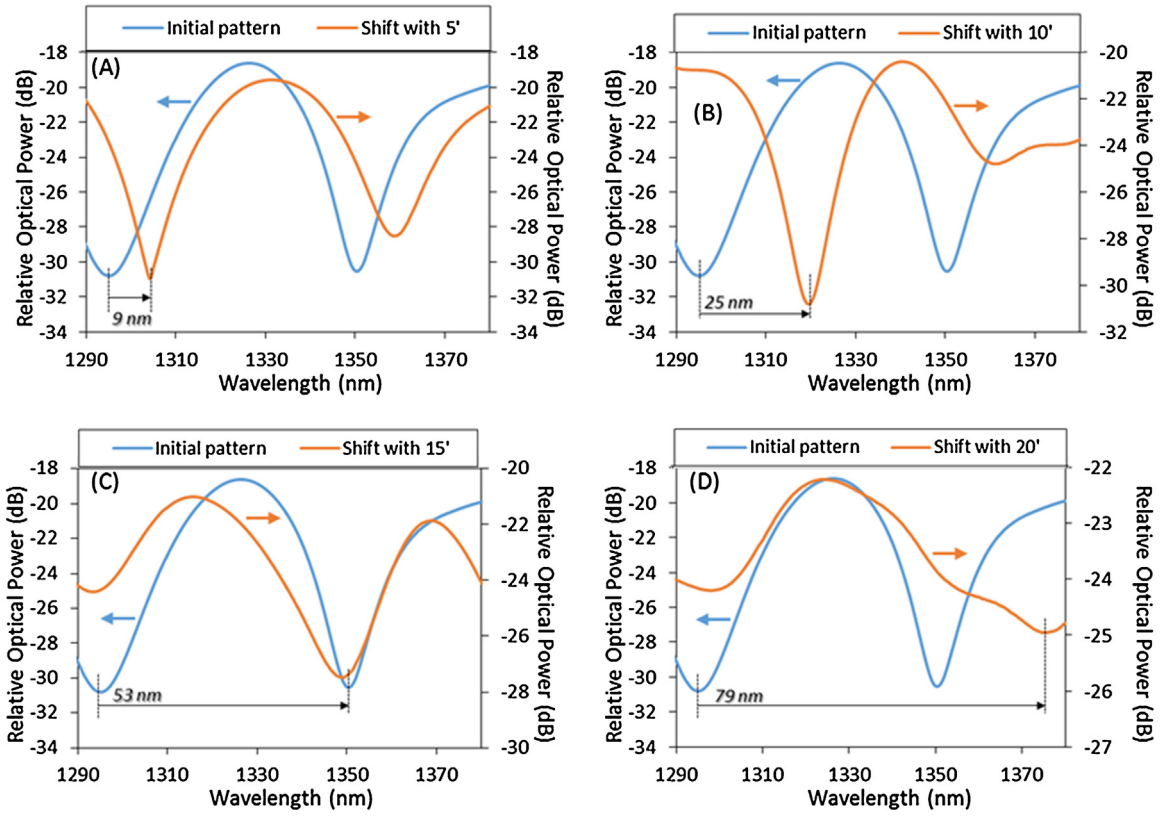

Fig. 6. Spectral red shift of an interferometric valley centered at 1295 nm along the sputtering: (A) 5′, (B) 10′, (C) 15′ and (D) 20′. In each case, initial pattern is in blue (left vertical axis) and the shifted one in orange (right vertical axis). (For interpretation of the references to colour in this figure legend, the reader is referred to the web version of this article.)

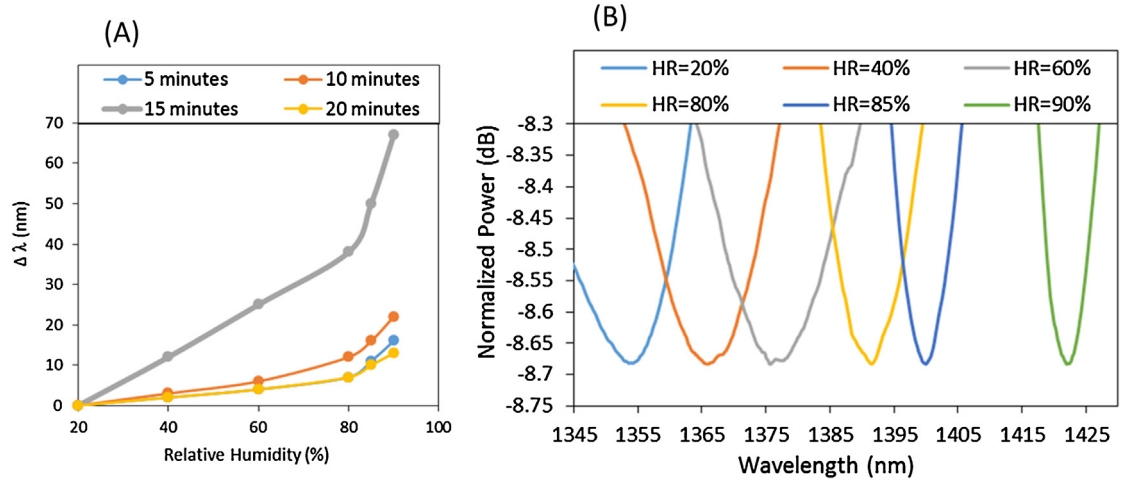

Fig. 7. (A) Wavelength shift for different relative humidity registered from the optimized sensor; (B) Detailed red shift of a certain transmission valley from the sensor with the highest sensitivity. All the spectra are normalized for the sake of clarity. (For interpretation of the references to colour in this figure legend, the reader is referred to the web version of this article.)

above and it is due to the nearby presence of LMR which makes the interference pattern disappear, worsening the response of the sensor. Taking into account that the main phenomenon of interaction between SnO_2 and H_2O molecules is the physisorption [27] and as it is explained and studied in [36], the response and recovery times of sensors with thinnest films are supposed to be faster.

Fig. 7B shows the detailed spectra centered at the transmission valley used as reference of the best sensor obtained for different values of RH. The sensor showed a red shift due to the effect of the humidity on the thin film [37]. All the spectra in the figure were normalized for the sake of clarity. Furthermore, it can be appreciated that when the RH is high, close to 80%, the spectra shift was also higher (with a sensitivity of 3 nm/%HR) than the spectra shift at lower RH values (from 20% to 80% HR the sensitivity was ~1 nm/%HR). In the range 80% –90% HR, the behavior of the sensor can be considered as exponential behavior. This result is very interesting because the sensor can be used in applications which a high

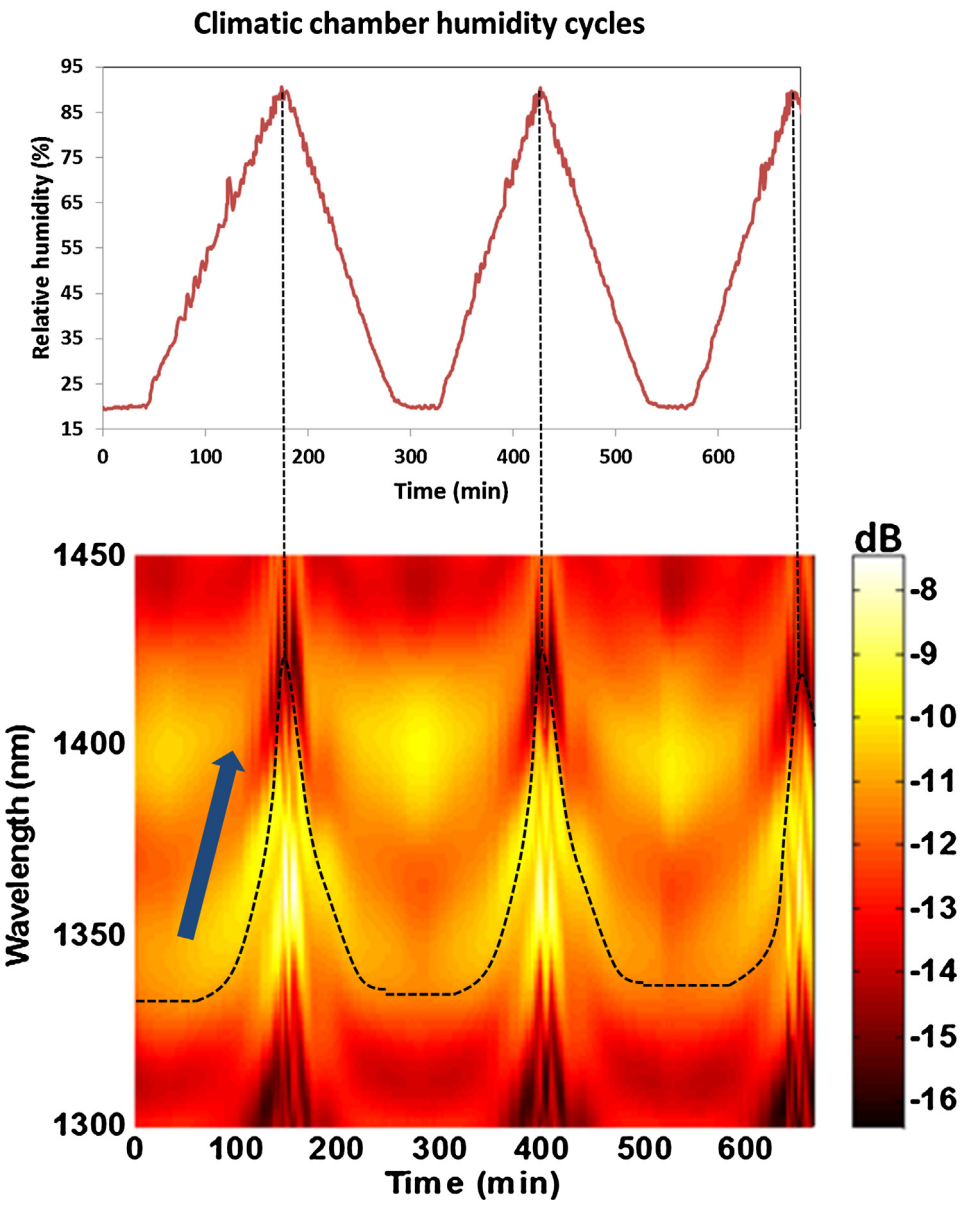

Fig. 8. (Up) Humidity cycles performed by the climatic chamber which the relative humidity is increased from 20% to 90% RH; (Down) Transmission spectra of the sensor when it was placed in the climatic chamber. The Y axis represented wavelength and the X axis time. The black dashed line represents the wavelength shift of the sensor with a nanofilm thickness of 1150 nm.

relative humidity is required to work. Also, due to the features of the sensor, the risk of short circuit with these conditions is avoided.

The response of the optimized sensor was studied with more detail by plotting the complete spectral evolution during different humidity conditions on real time by sampling the transmission spectra every minute: specifically, the device was exposed to changes between 20% and 90% HR three times. The results obtained are displayed in Fig. 8: the graph above shows the temporal evolution of relative humidity, whereas the spectra registered along the test are shown in the graph below. In this manner, the horizontal axis of the spectra graph, although expressed in time units, is directly related with the relative humidity value. It can be observed how the spectral shift follows the change in humidity along time: actually, the higher sensitivity above 80% is also noticeable. Furthermore, no hysteresis is observed and what is more, the response of the sensor is repetitive and stable in time (there is no shift when relative humidity is 20% between the cycles).

The temperature effect on the sensor under study was also checked: it has been studied using the same climatic chamber as before but was increased from 15 °C to 40 °C, setting the RH at 40%. Furthermore, the stability of the sensor towards temperature was studied with a cycle of 200 min at constant temperature (40 °C) once this value was reached. As it can be observed in Fig. 9, the wavelength shift of the peak was below 1 nm, which can be mathematically compensated.

5. Conclusions

Thanks to the study that it has been carried out in this paper, these conclusions can be derived. Firstly, oxide metallic (in our case SnO_2) can be use as sensing material in sensors based on an interferometric pattern. Also, this kind of materials can be work at room temperature which is a high advantage over other devices such as electronic sensors.

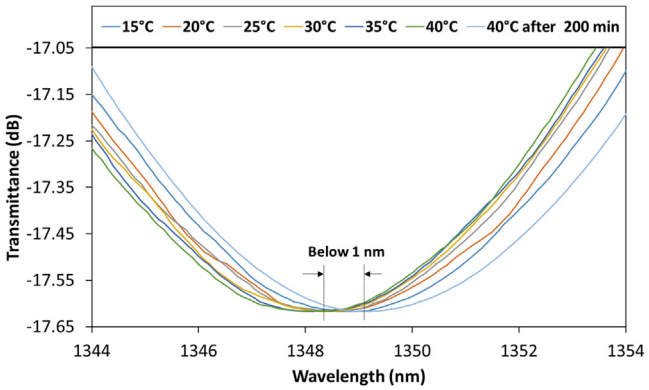

Fig. 9. Study of the wavelength shift of the selected peak of the sensor with a nanofilm of 1150 nm when it was exposed to different temperatures.

Whit the aim to obtain the best sensitivity for the sensors, it has been confirmed that the nanofilm thickness is the key parameter in this process. But to achieve it, it is necessary to work at nanometer scale, where nanofilm thickness is below the penetration depth of the evanescent field. The sputtering technique allows to work at this scale making very interesting its use in this work.

The operating mechanism of the sensor is based on the interaction between cladding modes and the SnO_2 nanofilm. To make it possible, a suitable nanofilm has to be deposited along the PCF-I. This study concludes that there is an optimal thickness, 1150 nm, and higher or lower thicknesses worsen the sensitivity of the sensor. It has been found that there is a tradeoff related with this parameter: as it increases, the interaction between cladding modes and nanofilm also increases but when the thickness reaches the value of the evanescent field, the device loses sensibility as the film grows. Moreover, during the construction process of the nanofilm another phenomenon occurs, the presence of magnetic resonances (LMR) which have to be avoided.

Due to the features of the PCF-I spectrum, the sensors were characterized by following the wavelength shifts. These measurements were robust and they allowed to control the nanofilm construction process as well as the characterization of the sensor.

To summarize, the resulting sensor offers a repeatable response, good repeatability in terms of thickness, low hysteresis, long-term stability and a humidity resolution of 0.067%HR. Taking these results account, this paper encourages to continue studying the construction of nanofilms based on metallic oxide to develop fiber optic sensors.

Competing interests

The authors declare that they have no competing interests.

Acknowledgments

This work was supported by the Spanish Economy and Competitivity Ministry-FEDERTEC2013-43679-R as well as Public University of Navarre grant program. The authors would like to express their gratitude to Nadetech Inc. for the design, fabrication and tune-up of the robot used for the deposition of the nanocoatings.

References

[1] R.C. Jorgenson, S.S. Yee, A fiber-optic chemical sensor based on surface plasmon resonance, Sens. Actuators B: Chem. 12 (1993) 213–220, http://dx.doi.org/10.1016/0925-4005(93)80021-3.
[2] B. Lee, Review of the present status of optical fiber sensors, Opt. Fiber Technol. 9 (2003) 57–79, http://dx.doi.org/10.1016/S1068-5200(02)00527-8.
[3] J. Ascorbe, J.M. Corres, F.J. Arregui, I.R. Matias, Optical fiber current transducer using lossy mode resonances for high voltage networks, J. Light Technol. 33 (2015) 2504–2510, http://dx.doi.org/10.1109/JLT.2015.2396353.
[4] P. Zubiate, C.R. Zamarre, I. Del Villar, I.R. Matias, S. Member, F.J. Arregui, Experimental Study and Sensing Applications of Polarization-Dependent Lossy Mode Resonances Generated by D-Shape Coated Optical Fibers, J. Lightwave Technol. 33 (2015) 2412–2418.
[5] P. Russell, Photonic crystal fibers, Science 80 (2003) 299 (358 LP-362) http://science.sciencemag.org/content/299/5605/358.abstract.
[6] Y.L. Hoo, W. Jin, C. Shi, H.L. Ho, D.N. Wang, S.C. Ruan, Design and modeling of a photonic crystal fiber gas sensor, Appl. Opt. 42 (2003) 3509, http://dx.doi.org/10.1364/ao.42.003509.
[7] K. Suzuki, H. Kubota, S. Kawanishi, M. Tanaka, M. Fujita, Optical properties of a low-loss polarization-maintaining photonic crystal fiber, Opt. Express 9 (2001) 676–680, http://dx.doi.org/10.1364/OE.9.000676.
[8] J.B. Jensen, L.H. Pedersen, P.E. Hoiby, L.B. Nielsen, T.P. Hansen, J.R. Folkenberg, J. Riishede, D. Noordegraaf, K. Nielsen, A. Carlsen, A. Bjarklev, Photonic crystal fiber based evanescent-wave sensor for detection of biomolecules in aqueous solutions, Opt. Lett. 29 (2004) 1974–1976, http://dx.doi.org/10.1364/OL.29.001974.
[9] J. Villatoro, M.P. Kreuzer, R. Jha, V.P. Minkovich, V. Finazzi, G. Badenes, V. Pruneri, Photonic crystal fiber interferometer for chemical vapor detection with high sensitivity, Opt. Express 17 (2009) 1447, http://dx.doi.org/10.1364/oe.17.001447.
[10] A. Lopez-Aldaba, A. Pinto, M. Lopez-Amo, O. Frazão, J. Santos, J. Baptista, H. Baierl, J.-L. Auguste, R. Jamier, P. Roy, Experimental and numerical characterization of a hybrid Fabry-Pérot cavity for temperature sensing, Sensors 15 (2015) 8042–8053, http://dx.doi.org/10.3390/s150408042.
[11] J. Villatoro, V. Finazzi, V.P. Minkovich, V. Pruneri, G. Badenes, Temperature-insensitive photonic crystal fiber interferometer for absolute strain sensing, Appl. Phys. Lett. 91 (2007) 89–92, http://dx.doi.org/10.1063/1.2775326.
[12] P. Hu, X. Dong, K. Ni, L.H. Chen, W.C. Wong, C.C. Chan, Sensitivity-enhanced Michelson interferometric humidity sensor with waist-enlarged fiber bitaper, Sens. Actuators B: Chem. 194 (2014) 180–184, http://dx.doi.org/10.1016/j.snb.2013.12.081.
[13] Y. Song, M. Hu, C. Wang, Z. Tian, Q. Xing, L. Chai, C. Wang, Environmentally Stable, High Pulse Energy Laser Operating in the Soliton-Like Regime, IEEE Photonics Technol. Lett. 20 (2008) 1088–1090.
[14] J. Shi, V.K.S. Hsiao, T.R. Walker, T.J. Huang, Humidity sensing based on nanoporous polymeric photonic crystals, Sens. Actuators B: Chem. 129 (2008) 391–396, http://dx.doi.org/10.1016/j.snb.2007.08.037.
[15] S. Zheng, Y. Zhu, S. Krishnaswamy, Fiber humidity sensors with high sensitivity and selectivity based on interior nanofilm-coated photonic crystal fiber long-period gratings, Sens. Actuators B: Chem. 176 (2013) 264–274, http://dx.doi.org/10.1016/j.snb.2012.09.098.
[16] W.H. Reeves, D.V. Skryabin, F. Biancalana, J.C. Knight, P.S.J. Russell, F.G. Omenetto, a Efimov, a J. Taylor, Transformation and control of ultra-short pulses in dispersion-engineered photonic crystal fibres, Nature 424 (2003) 511–515, http://dx.doi.org/10.1038/nature01798.
[17] L. Rindorf, J.B. Jensen, M. Dufva, L.H. Pedersen, P.E. Høiby, O. Bang, Photonic crystal fiber long-period gratings for biochemical sensing, Opt. Express 14 (2006) 8224–8231, http://dx.doi.org/10.1364/OE.14.008224.
[18] J. Mathew, Y. Semenova, G. Farrell, Experimental demonstration of a high-sensitivity humidity sensor based on an Agarose-coated transmission-type photonic crystal fiber interferometer, Appl. Opt. 52 (2013) 3884–3890, http://dx.doi.org/10.1364/AO.52.003884.
[19] D. Lopez-Torres, C. Elosua, J. Villatoro, J. Zubia, M. Rothhardt, K. Schuster, F.J. Arregui, Photonic crystal fiber interferometer coated with a PAH/PAA nanolayer as humidity sensor, Sens. Actuators B: Chem (2016), http://dx.doi.org/10.1016/j.snb.2016.09.144.
[20] D. Lopez-Torres, C. Elosua, M. Hernaez, J. Goicoechea, F.J. Arregui, From superhydrophilic to superhydrophobic surfaces by means of polymeric layer-by-layer films, Appl. Surf. Sci. 351 (2015) 1081–1086, http://dx.doi.org/10.1016/j.apsusc.2015.06.004.
[21] B. Jaffe, R.S. Roth, S. Marzullo, Properties of piezoelectric ceramics in the solid-solution series lead titanate-lead zirconate-lead oxide: tin oxide and lead titanate-lead hafnate, J. Res. Natl. Bur. Stand. 1934 55 (1955) 239–254, http://dx.doi.org/10.6028/jres.055.028.
[22] Q. Kuang, C. Lao, L.W. Zhong, Z. Xie, L. Zheng, High-sensitivity humidity sensor based on a single SnO2 nanowire, J. Am. Chem. Soc. 129 (2007) 6070–6071, http://dx.doi.org/10.1021/ja070788m.
[23] J. Ascorbe, C. Sanz, J.M. Corres, F.J. Arregui, I.R. Matias, S.C. Mukhopadhyay, High sensitivity extrinsic Fabry-Pèrot interferometer for humidity sensing, Proc. Int. Conf. Sens. Technol. (2016) 143–146, http://dx.doi.org/10.1109/ICSensT.2015.7438380, ICST. 2016–March (2016).
[24] E. Shanthi, V. Dutta, A. Banerjee, K.L. Chopra, Electrical and optical properties of undoped and antimony-doped tin oxide films, J. Appl. Phys. 51 (1980) 6243–6251, http://dx.doi.org/10.1063/1.327610.
[25] K. Maier, A. Helwig, G. Müller, P. Hille, M. Eickhoff, Effect of water vapor and surface morphology on the low temperature response of metal oxide semiconductor gas sensors, Mater. (Basel) 8 (2015) 6570–6588, http://dx.doi.org/10.3390/ma8095323.
[26] W. Schmid, Consumption Measurements on SnO 2 Sensors in Low and Normal Oxygen Concentration, Diss. Am Inst. Für Chemie Und Pharm. Der Eberhard-Karls- Univ. Tübingen, 2004.

[27] W.E. Pickett, Electronic structure of the high-temperature oxide superconductors, Rev. Mod. Phys. 61 (1989) 433–512, http://dx.doi.org/10.1103/RevModPhys.61.433.
[28] J. Mathew, Y. Semenova, G. Rajan, G. Farrell, Humidity sensor based on photonic crystal fibre interferometer, Electron. Lett. 46 (2010) 1341, http://dx.doi.org/10.1049/el.2010.2080.
[29] E. Udd, W.B. Spillman, Fiber Optic Sensors Fiber Optic Sensors An Introduction for Engineers and Scientists, A John Wiley Sons, Ltd Publ., 2011, pp. 498.
[30] O. Letters, Refractometry based on a photonic crystal ber interferometer, Opt. Lett. 34 (2009) 617–619.
[31] I. Del Villar, C.R. Zamarreño, M. Hernaez, P. Sanchez, F.J. Arregui, I.R. Matias, Generation of surface plasmon resonance and lossy mode resonance by thermal treatment of ITO thin-films, Opt. Laser Technol. 69 (2015) 1–7, http://dx.doi.org/10.1016/j.optlastec.2014.12.012.
[32] C.R. Zamarreño, M. Hernáez, I. Del Villar, I.R. Matías, F.J. Arregui, Optical fiber pH sensor based on lossy-mode resonances by means of thin polymeric coatings, Sens. Actuators B: Chem. 155 (2011) 290–297, http://dx.doi.org/10.1016/j.snb.2010.12.037.
[33] P. Zubiate, C.R. Zamarreño, I. Del Villar, I.R. Matias, F.J. Arregui, High sensitive refractometers based on lossy mode resonances (LMRs) supported by ITO coated D-shaped optical fibers, Opt. Express 23 (2015) 8045, http://dx.doi.org/10.1364/oe.23.008045.
[34] J. Mathew, Y. Semenova, G. Farrell, Effect of coating thickness on the sensitivity of a humidity sensor based on an Agarose coated photonic crystal fiber interferometer, Opt. Express 21 (2013) 6313–6320, http://dx.doi.org/10.1364/OE.21.006313.
[35] J. Mathew, Y. Semenova, G. Farrell, A high sensitivity humidity sensor based on an Agarose coated photonic crystal fiber interferometer, Proceedings of SPIE, 8421 (2012) 842177–842177-4, 10.1117/12.975153.
[36] C. Liewhiran, S. Phanichphant, Influence of thickness on ethanol sensing characteristics of doctor-bladed thick film from flame-made ZnO nanoparticles, Sensors 7 (2007) 185–201, http://dx.doi.org/10.3390/s7020185.
[37] J. Ascorbe, J.M. Corres, I.R. Matias, F. Arregui, High sensitivity humidity sensor based on cladding-etched optical fiber and lossy mode resonances, Sens. Actuators B: Chem. 233 (2016) 7–16, http://dx.doi.org/10.1016/j.snb.2016.04.045.

Biographies

Diego López-Torres received the M.S. degree in electrical and electronic engineering and the master's degree in communications from the Public University of Navarra (UPNA), Pamplona, Spain, in 2013 and 2014, respectively. Since 2014, he has been working as a Researcher at the UPNA. In 2105, he obtained a scholarship from this university. His research interest includes optical fiber sensors, photonic crystal fiber and nanostructured materials.

Cesar Elosúa Aguado received his MS degree in electrical and electronic engineering from the Public University of Navarre (UPNA, Pamplona, Spain) in 2004. In the same year, he obtained a scholarship from the Science and Technology Spanish Ministry and he joined the optical fiber sensor group at UPNA. During 2008, he was a visiting Ph.D. student at the University of Limerick and at the City University of London. He became a lecturer of this department in 2009, receiving his PhD degree in the next year. His research interests include optical fiber sensors and networks, organometallic chemistry and data mining techniques.

Joel Villatoro received the M.Sc. and Ph.D. degrees in optics from the National Institute for Astrophysics, Optics, and Electronics, Puebla, Mexico, in 1995 and 1999, respectively. He is currently Ikerbasque Research Professor at the University of the Basque Country, Spain. Prior to that, he worked for the Aston Institute of Photonic Technologies (UK) and the world-famous ICFO –Institute of Photonic Sciences (Spain), among others. He is the author of nearly 100 scientific publications and of 6 patents. His contributions to his field are acknowledged by the internationally community as reflected by a large number of citations and several invited talks.

Joseba Zubia received a degree in solid-state physics in 1988 and the PhD degree in physics from the University of the Basque Country, in 1993. His PhD work focused on optical properties of ferroelectric liquid crystals. He is a full professor at the Telecommunications Engineering School (University of the Basque Country, Bilbao, Spain). He has more than 8 years of experience doing basic research in the field of plastic optical fibers. At present, he is involved in research projects in collaboration with universities and companies from Spain and other countries in the field of plastic optical fibers, fiber-optic sensors, and liquid crystals. Prof. Zubia won a special award for best thesis in 1995.

Manfred Rothhardt received his diploma degree from the Physics faculty of the Friedrich-Schiller-University, Jena, Germany in 1984. From 1984–1991 he was a scientific assistant in the research center of Carl-Zeiss-Jena GmbH. From 1991–1995 he was with Jenoptik AG leading a R&D group developing interferometric measurement systems. Since 1995 he is with Institute of Photonic Technology, Jena. His research interest includes applications of fiber Bragg gratings and planar lightwave circuits in sensors, biophotonics, fiber lasers and telecommunication.

Kay Schuster holds the group leader position of the Optical Fibres Technology Group within the Fibre Optics Division of the Leibniz Institute of Photonic Technology (IPHT Jena). He obtained his PhD in inorganic chemistry 1995 at the University of Karlsruhe (Research University). Dr. Kay Schuster is engaged for many years in preparation of specialty fibers, based on heavy metal oxide glasses, chalcogenide glasses and high purity silica. The recent activities of Dr. Schuster are concentrated on design and preparation of special functionalized microstructured fibers for passive, active and remote sensing applications. Beside the fabrication of specialty microstructured fibers the group is intensively engaged in material science as well as preform and fiber manufacturing for high power fiber lasers and FBG and Raman based sensing applications. He has coauthored/authored 82 articles in refereed journals, 2 book chapters and holds 3 patents.

Francisco J. Arregui (M'01) is a Full Professor at the Public University of Navarre, Pamplona, Spain. He was part of the team that fabricated the first optical fiber sensor by means of the Layer-by-Layer assembly method at Virginia Tech, Blacksburg, VA, USA, in 1998. He is the author of around 300 scientific journal and conference publications. He has been an Associate Editor of "IEEE Sensors Journal", "Journal of Sensors" (founded by Prof, Arregui in 2007), and "International Journal on Smart Sensing and Intelligent Systems". He is also the editor of the books entitled Sensors-Based on Nanostructured Materials and Optochemical Nanosensors.